Indoor Positional Tracking Using Dual-Axis Rotating Laser Sweeps

Shahidul Islam, Bogdan Ionescu
Mgestyk Technologies Inc.
Ottawa, Ontario, Canada
shahid, bogdan@mgestyk.com

Cristian Gadea, Dan Ionescu
School of Electrical Engineering and Computer Science
University of Ottawa
Ottawa, Ontario, Canada
cgadea, dan@ncct.uottawa.ca

***Abstract*—Accurate positioning of objects within an indoor environment is essential for applications such as virtual reality, robotics and multirotor drones. Previous methods of obtaining six-degrees-of-freedom for a tracked object have been susceptible to latency and accumulated error, computationally intensive, inaccurate, costly, or required exotic components, setups and calibration procedures. This paper presents a novel architecture and implementation of an indoor tracking system that consists of a rotary-laser base station and a tracked object equipped with photodiode sensors. The base station emits horizontal and vertical laser lines that sweep across the environment in sequence. The base station also emits an infrared synchronization beacon that floods the environment between each sweep. The tracked object consists of multiple photodiode sensors and a processing unit. Based on the timings between the synchronization beacons and the sweeps observed by each photodiode, along with the known configuration of the photodiode constellation, the position and orientation of the tracked object can be determined with high accuracy, low latency, and low computational overhead. In addition, the system allows a large number of such objects to be tracked within the same space, as each tracked object can be a separate embedded device. The Nikon iGPS tracking system, along with the more recently announced Lighthouse technology from Valve Corporation, use multiple base stations to triangulate a tracked object, while we will show that one is sufficient for basic tracking. In addition, this paper is the first to describe the specifications for a low-cost version of such a system. Observations and performance characteristics of the constructed prototypes are discussed.**

***Index Terms*—indoor positioning, localization, angle measurement, laser beacon, infrared sensor, positioning, orientation, triangulation**

I. Introduction

Location sensing systems are presently witnessing increased attention from the research community due to the advent of new virtual reality (VR) head-mounted displays (HMDs) and input devices from companies such as Oculus, HTC/Valve and Sony. In research literature, these are also known as indoor location or positioning systems. Accurate tracking systems are in big demand and many researchers from academia and industry are currently engaged in researching a variety of approaches to this localization problem. One of the major challenges of VR systems is related to placing the user into the VR world, thereby merging the VR and the real world of the user in the same geometric representation. For example, how the user's hand or body is displayed in the virtual world (along with its 3D rendered objects, actions, and scenes) has to be consistent with the real world. There have been various attempts at solving this problem, and it stems in geometrically projecting the real-world space onto the virtual space with as little separation between the two as possible, i.e. connecting the axes of the 3D space to the same origin and using the same distance units. It is worth noting that even a small amount of error in the above operations has a negative effect on the user's perception of the two spaces, potentially leading to nausea as the user is disoriented due to the spatial desynchronization between their real movement and their virtually-represented movement.

To compensate for this effect, numerous implementations of positional tracking systems have been proposed in the literature. However, while there is large demand for an accurate and affordable low-latency six-degrees-of-freedom tracking system, there is still no such solution available on the consumer electronics market. In addition to VR, the industrial applications of such systems are numerous, spanning from location detection of products in warehouses, to location detection in hospitals of medical personnel, patients and equipment. Such tracking technology is also important for automation and robotics, including for autonomous robot or drone navigation of indoor environments.

In order to meet the low-latency requirements of VR and other applications, a tracking system should avoid CPU and I/O-intensive pose calculations whenever possible. The system described in this paper uses one base station that contains two rotors, one horizontal and one vertical. Each rotor contains a mirror and a line lens, thereby allowing a wide-angle horizontal and vertical fan of light to sweep across the real-world environment in sequence. A sync blinker on the base station is used to flood the environment with an infrared beacon. The tracked objects in the room use the synchronization beacon as a timing synchronization pulse, and by knowing the rotor revolution period, the photodiode receptors on the object surface can time the laser sweeps and determine their angle relative to the base station. The system proposed in this paper therefore distributes the pose calculation so that each tracked object performs its own angle computations with high temporal resolution, thereby resulting with high spatial resolution. Since each tracked object operates independently of the base station, multiple objects can be added and tracked within the scan volume of the base station. The base station

can be battery-operated as it does not require a host PC, thereby also simplifying the wiring.

The rest of this paper is organized as follows: Section II investigates the current state-of-the-art and how this work differs from it. Section III then presents the architecture of the proposed tracking system. Section IV describes the implementation details and tradeoffs that were made. The resulting tracking system is presented in section V. Finally, section VI reflects on the contributions of this paper and discusses future research.

II. Related Work

With the release of the Oculus Rift DK2 HMD for developers in 2014, Oculus revealed a low-cost positional tracking system that uses an infrared camera to track a constellation of infrared LEDs on the DK2 HMD [1]. Each individual LED (out of 40 total) is modulated in the time domain in such a way that visible LEDs can be uniquely identified after 10 frames are captured by the camera (each LED repeats a unique 10-bit pattern). The blinking of the tracking LEDs is synchronized to the shutter of the camera at 60Hz. The HMD is connected to the camera by a cable used for this purpose, and both devices are connected to a host PC. Based on the known geometric configuration of the LEDs on the HMD, and by using 2D images from the calibrated camera containing visible dots that identify each LED (which requires scanning through the entire image), the host PC then solves the perspective-n-point problem to obtain a 3D pose estimation for the HMD [2]. This process can be computationally demanding due to the large amount of pixel data that needs to be transmitted and processed, as greater tracking accuracy is achieved with greater image resolution and frame rate. It is therefore challenging to implement with current mobile or embedded devices without significant heat dissipation and power consumption challenges due to the constant high I/O and CPU requirements.

In addition to camera-based approaches, several other technologies have been used for indoor tracking, including Wi-Fi, RFID, ultrasonic, electromagnetic and tracking based on inertial measurement units (IMUs). A good survey of these approaches is available in [3]. This paper, however, will focus on tracking approaches that make use of photodiodes. Some of the earlier tracking work involving photodiodes was performed by Gruss et. al. [4], who successfully implemented a range-finding algorithm using light stripes detected by an array of photodiodes at 1000 frames per second. In 2007, Raskar et. al. [5] showed how the position and orientation of photodiode-based tags were determined by projecting various patterns and observing how they are detected by the photodiodes. The thesis of S. Linga used multiple transmitting laser modules to triangulate a mobile robot with a square pyramid-shaped tracked object containing four photodiodes, one per triangular side [6].

In the late 1990s, the company Arc Second developed the "indoor Global Positioning System" (iGPS). This technology was acquired by Metris in 2006 and later by Nikon Metrology in 2009 [7]. The system uses a one-axis rotary-laser base station to project two fanned laser beams in a "V" shape. It also emits an infrared sync signal to indicate the start of every revolution of the rotor. Tracked objects containing two photodiode sensors can then be placed within a scan volume. Each photodiode uses the sync signal to begin its timing to the two laser sweeps. The "V" configuration of the laser lines allows the elevation to be calculated based on the time between the sweeps (a higher elevation, and therefore a higher position in the "V", is indicated by a longer time between the sweeps). Azimuth is calculated by using the time indicated by the midpoint between the two laser sweep pulses. The angular data for the two photodiodes is then reported to a workstation via Ethernet. While the single-rotor design simplifies the base station, at least two base stations are required in order to triangulate the two-sensor tracked object, and the distance between the base stations must be established through a calibration process. The price for an iGPS system is said to be "around $180,000" [6]. Several academic works have analyzed the functionality and performance of iGPS [8][9].

In March 2015, Valve Corporation announced a technology called "Lighthouse" for tracking VR head mounted displays and input devices. Lighthouse uses two dual-axis base stations [10], and the base station design is similar to the one proposed in this paper. The technical specifications of Lighthouse are not yet published, however, and many details about the system (synchronization method between base stations, calibration procedure etc.) remain unclear. The system proposed in this paper focuses on a single base station design and a three-sensor tracked object.

III. Architecture

The architecture of the proposed tracking system consists of two key components: a base station and a tracked object. The base station contains the sync blinker and the rotation mechanisms that produce the horizontal and vertical laser sweeps. The tracked object contains multiple photodiodes, each of which will individually pick up the signals from the base station and use them to determine their azimuth and elevation angles relative to the base station. In addition, the tracked object transmits its angle data to a host PC, which is responsible for calculating the 3D position and orientation of the object by using a tracking algorithm.

A. Base Station Architecture

As shown in Figure 1, the base station consists of several key components. The sync blinker is denoted by B_1, the rotors by R_1 and R_2, and the lasers by L_1 and L_2.

Light from the laser unit L_1 is reflected off a mirror and a line lens arrangement placed on a base plate attached to a motor. The base plate and motor are shown together as rotor R_1. This rotor rotates counterclockwise. Thus rotor R_1 moves the vertical laser scan line from position S_1S_2 at t_1 to $S_1^{'}S_2^{'}$ at t_2. The vertical laser line swept by rotor R_1 in the scan volume will be used to obtain the azimuth angle measurement of the receiving sensor on the tracked object.

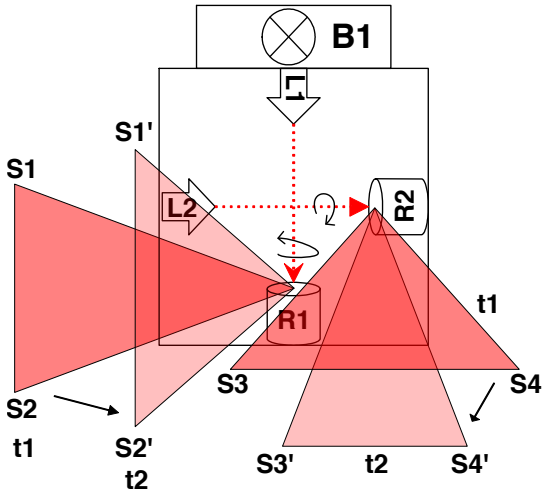

Fig. 1. Base station design.

Similarly, light from laser L_2 is reflected off of the optical arrangement of rotor R_2. Rotor R_2 rotates clockwise, thereby moving a horizontal laser scan line from position S_3S_4 at t_1 to position $S_3^{'}S_4^{'}$ at t_2. The horizontal laser line swept by rotor R_2 in the scan volume will be used to obtain the elevation angle measurement of the receiving sensor on the tracked object. The sync blinker B_1 floods the scan volume with a global beacon. It sends out frequency-modulated pulses when the laser line from rotor R_1 is at $0°$ azimuth angle and when the laser line from rotor R_2 is at $0°$ elevation angle (pointing upwards). Both rotors R_1 and R_2 are rotated at the same RPM but their relative phase is $180°$. This means that when the laser line from rotor R_1 is at $0°$ azimuth angle, the laser line from rotor R_2 is at at $180°$ elevation angle (pointing downward). The different rotor phases ensure that the scan volume is scanned by the vertical and the horizontal laser lines in an alternating fashion. The speed and the phase of the rotors is controlled by a microcontroller on the base station.

B. Tracked Object Architecture

The tracked object in the scan volume consists of a constellation of photodiodes whose geometry is known. The signal from a photodiode is passed through an analog front-end circuit that conditions the signal by removing the DC component and amplifying only the frequency components of interest. The final stage of the analog processing consists of a high-speed comparator that converts the signal received by the photodiode into logic levels, which are used by a processing unit to determine the azimuth and elevation of each connected photodiode. The processing unit then transfers the obtained angle values to the host PC.

A representation of the signal or pulse train received by a photodiode from the base station is shown in Figure 2. Pulses P_1 and P_2 are the sync blinker pulses emitted by B_1 when the azimuth angle is $0°$ for the vertical laser line of rotor R_1. These two pulses, P_1 and P_2, are simultaneously received by all photodiodes on the tracked object that make up a constellation.

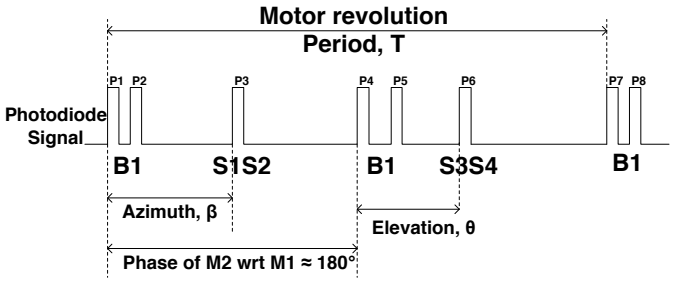

Fig. 2. Sample pulse train received by a photodiode on a tracked object. Distances between pulses are not to scale.

Pulse P_3 is received by a photodiode when the vertical laser scan line S_1S_2 passes it. The time between the rising edges of the pulse P_1 and P_3 gives a direct measurement of the azimuth angle of the photodiode in the target constellation. Pulses P_4 and P_5 are emitted by the sync blinker B_1 when the elevation angle is $0°$ (pointing upward) for the horizontal laser line of the base-plate of rotor R_2. Pulse P_6 is received by the photodiode when the horizontal laser line S_3S_4 passes it. The time between the rising edge of pulse P_4 and P_6 gives a direct measurement of the elevation angle of the photodiode. Pulses P_7 and P_8 emitted by B_1 are the same as P_1 and P_2, indicating the start of a new revolution of rotor R_1. The time between the rising edge of pulse P_1 and P_7 provides the rotor revolution period, T.

The processing unit computes the azimuth and elevation angles for each photodiode as follows:

$$Azimuth,\beta = \left(\frac{time(P_3) - time(P_1)}{T}\right) \times 360° \quad (1)$$

$$Elevation,\theta = \left(\frac{time(P_6) - time(P_4)}{T}\right) \times 360° \quad (2)$$

The time between P_1 and P_2, and the time between P_4 and P_5 are much shorter than depicted in Figure 2. The pulses P_1 and P_2 are emitted from the base station in such a way that the laser line pulse P_3 does not interfere with pulse P_1 or P_2. Likewise, pulses P_4 and P_5 are sent out from the base station in such a way that the laser line pulse P_6 does not interfere with P_4 or P_5.

Note that the sync blinker pulses P_1, P_2, P_4, and P_5 are received simultaneously by all photodiodes of a constellation. In order to measure the time of such simultaneous pulse events, the processing unit should be implemented by using a field-programmable gate array (FPGA) or a microcontroller with auto hardware timing-capture functionality.

C. Position and Orientation Computation

Figure 3 shows the photodiode sensor constellation ABC. The projection of the sensor constellation ABC on the XY plane is A'B'C'.

Let $\overrightarrow{R_A}, \overrightarrow{R_B}$, and $\overrightarrow{R_C}$ be the location vectors representing the photodiode sensors at A (x_A, y_A, z_A), B (x_B, y_B, z_B), and C (x_C, y_C, z_C) respectively.

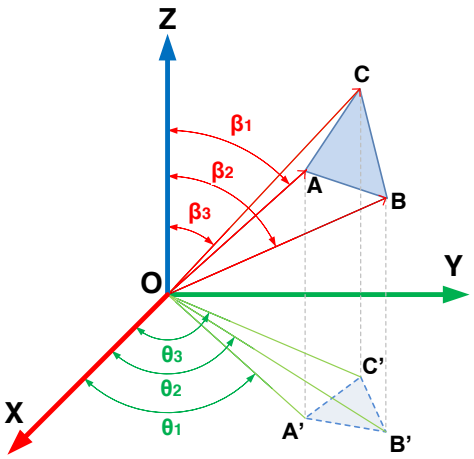

Fig. 3. Sensor constellation ABC in Cartesian coordinates.

According to the Spherical coordinate system (range, azimuth, and elevation), photodiodes A, B, and C will be located with (R_A, θ_1, β_1), (R_B, θ_2, β_2), and (R_C, θ_3, β_3).

The azimuth (θ) and the elevation (β) angles are measured with the help of the base station. The ranges of the sensors are calculated by solving a system of non-linear equations derived next.

For a sensor in the constellation at (x, y, z) with the range $\left|\overrightarrow{R}\right|$, azimuth θ, and elevation β, the following can be derived:

$$x = \left|\overrightarrow{R}\right| sin(\beta)cos(\theta) \tag{3}$$

$$y = \left|\overrightarrow{R}\right| sin(\beta)sin(\theta) \tag{4}$$

$$z = \left|\overrightarrow{R}\right| cos(\beta) \tag{5}$$

Let the angles between vectors $\overrightarrow{R_A}$ and $\overrightarrow{R_B}$, $\overrightarrow{R_B}$ and $\overrightarrow{R_C}$, and $\overrightarrow{R_A}$ and $\overrightarrow{R_C}$ be α_{AB}, α_{BC}, and α_{AC} respectively.

According to the dot product rule,

$\overrightarrow{R_A}.\overrightarrow{R_B} = (x_A\hat{i} + y_A\hat{j} + z_A\hat{k}).(x_B\hat{i} + y_B\hat{j} + z_B\hat{k})$

Or,

$$\left|\overrightarrow{R_A}\right| . \left|\overrightarrow{R_B}\right| cos\alpha_{AB} = x_A x_B + y_A y_B + z_A z_B \tag{6}$$

In the above equation,

$$x_A x_B = \left|\overrightarrow{R_A}\right| sin\beta_1 cos\theta_1 \left|\overrightarrow{R_B}\right| sin\beta_2 cos\theta_2 \tag{7}$$

$$y_A y_B = \left|\overrightarrow{R_A}\right| sin\beta_1 sin\theta_1 \left|\overrightarrow{R_B}\right| sin\beta_2 sin\theta_2 \tag{8}$$

$$z_A z_B = \left|\overrightarrow{R_A}\right| cos\beta_1 \left|\overrightarrow{R_B}\right| cos\beta_2 \tag{9}$$

Following can be derived by using the equations 7, 8, and 9 into equation 6:

$$cos\alpha_{AB} = sin\beta_1 cos\theta_1 sin\beta_2 cos\theta_2 + sin\beta_1 sin\theta_1 sin\beta_2 sin\theta_2 + cos\beta_1 cos\beta_2 \tag{10}$$

$cos\alpha_{AB}$ in the above equation can be calculated as all the azimuth (θ) and elevation (β) angles are known at time when the measurements are taken from the tracking system. Similarly, $cos\alpha_{BC}$ and $cos\alpha_{AC}$ can be derived into the following forms:

$$cos\alpha_{BC} = sin\beta_2 cos\theta_2 sin\beta_3 cos\theta_3 + sin\beta_2 sin\theta_2 sin\beta_3 sin\theta_3 + cos\beta_2 cos\beta_3 \tag{11}$$

$$cos\alpha_{AC} = sin\beta_1 cos\theta_1 sin\beta_3 cos\theta_3 + sin\beta_1 sin\theta_1 sin\beta_3 sin\theta_3 + cos\beta_1 cos\beta_3 \tag{12}$$

The following system of non-linear equations for the unknown range variables R_A, R_B, and R_C can be written by applying the law of cosines in triangle OAB, OBC, and OAC:

$$f(R_A, R_B) = R_A^2 + R_B^2 - 2R_A R_B\, cos\alpha_{AB} - AB^2 = 0 \tag{13}$$

$$f(R_B, R_C) = R_B^2 + R_C^2 - 2R_B R_C\, cos\alpha_{BC} - BC^2 = 0 \tag{14}$$

$$f(R_A, R_C) = R_A^2 + R_C^2 - 2R_A R_C\, cos\alpha_{AC} - AC^2 = 0 \tag{15}$$

The length of the sides AB, BC, and AC of the constellation are known in advance. Above system of equations are solved simultaneously for R_A, R_B, and R_C using Newton's root finding method. To apply Newton's method, the Jacobian matrix is formed as follows:

$$\mathfrak{J}(R_A, R_B, R_C) = \begin{bmatrix} \frac{\partial f(R_A,R_B)}{\partial R_A} & \frac{\partial f(R_A,R_B)}{\partial R_B} & \frac{\partial f(R_A,R_B)}{\partial R_C} \\ \frac{\partial f(R_B,R_C)}{\partial R_A} & \frac{\partial f(R_B,R_C)}{\partial R_B} & \frac{\partial f(R_B,R_C)}{\partial R_C} \\ \frac{\partial f(R_A,R_C)}{\partial R_A} & \frac{\partial f(R_A,R_C)}{\partial R_B} & \frac{\partial f(R_A,R_C)}{\partial R_C} \end{bmatrix} \tag{16}$$

Or, $\mathfrak{J}(R_A, R_B, R_C) =$

$$\begin{bmatrix} 2R_A - 2R_B\, cos\alpha_{AB} & 2R_B - 2R_A\, cos\alpha_{AB} & 0 \\ 0 & 2R_B - 2R_C\, cos\alpha_{BC} & 2R_C - 2R_B\, cos\alpha_{BC} \\ 2R_A - 2R_C\, cos\alpha_{AC} & 0 & 2R_C - 2R_A\, cos\alpha_{AC} \end{bmatrix} \tag{17}$$

Initially, at iteration step 0 ($k = 0$), a set of random numbers are assigned to the solution vector $[R_{A_0}\ R_{B_0}\ R_{C_0}]^T$. Iteration steps are advanced using the following equation at any step k:

$$\begin{bmatrix} R_{A_{k+1}} \\ R_{B_{k+1}} \\ R_{C_{k+1}} \end{bmatrix} = \begin{bmatrix} R_{A_k} \\ R_{B_k} \\ R_{C_k} \end{bmatrix} - \mathfrak{J}^{-1}(R_{A_k}, R_{B_k}, R_{C_k}). \begin{bmatrix} f(R_{A_k}, R_{B_k}) \\ f(R_{B_k}, R_{C_k}) \\ f(R_{A_k}, R_{C_k}) \end{bmatrix} \tag{18}$$

Iteration steps are stopped when a maximum preset number of iterations are performed or when the solution error is within a given tolerance (whichever is reached the earliest). When a solution is found for R_A, R_B, and R_C at step k, it is expected that following will hold true:

$$\begin{bmatrix} f(R_{A_k}, R_{B_k}) \\ f(R_{B_k}, R_{C_k}) \\ f(R_{A_k}, R_{C_k}) \end{bmatrix} \approx \begin{bmatrix} 0.0 \\ 0.0 \\ 0.0 \end{bmatrix} \tag{19}$$

For more than 3 sensors in the constellation, the number of non-linear equations can be more than the number of photodiodes. In such cases, Gauss-Newton's method can be applied to find the solution vector with the least mean square (LMS) error.

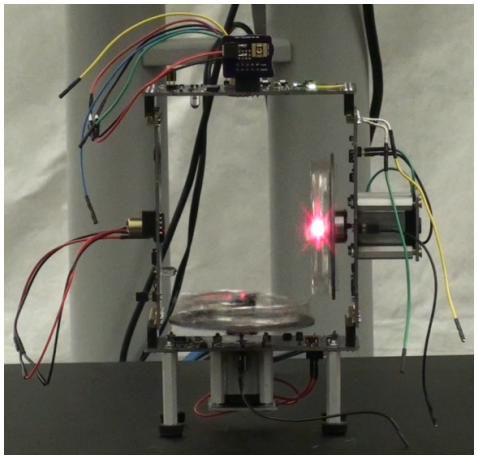

Fig. 4. Implemented base station.

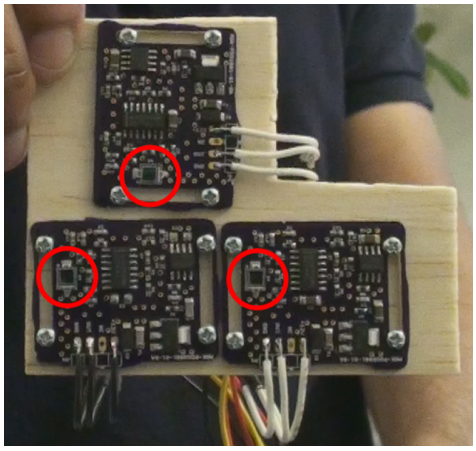

Fig. 5. Tracked object consisting of three photodiode sensor boards. The photodiodes are circled in red.

IV. Implementation

The architecture described in Section III was implemented into a functional prototype. One of the key objectives of the prototype was to use low-cost components in order to demonstrate that such a rotary-laser positional tracking system can be made affordable for consumers. In addition, the implementation was designed to be modular so that different components (lasers, rotors etc.) could be evaluated. Overall, the implementation consists of six different circuit boards (four for the base station, two for the tracked object) and three applications (base station firmware, tracked object firmware and host PC software).

A. Base Station Implementation

A photograph of the implemented base station running can be see in Figure 4. The walls of the base station consists of two laser boards and two motor boards. In addition, the sync blinker board and two circular rotor boards are present. The sync blinker board was implemented using a Osram SFH 4716S high intensity infrared LED.

As can be seen in the photo, 5mW red laser pointers were used as the laser source for development. Note how the red laser on the horizontal rotor faces towards the back when the vertical rotor's laser faces towards the front. To make this possible, two DC motors were used, and their RPM was measured through an additional infrared LED shining through holes in the rotors onto a photodiode beneath each rotor. A rotation frequency of 15Hz was found to be sufficient for testing. The entire base station is powered via a regular 12V power connector, which can be connected to a mobile battery pack.

B. Tracked Object Implementation

For the tracked object, a circuit board was designed to hold one photodiode along with its analog front-end circuit. Osram BPW34S-Z photodiodes were used for their relatively large surface area, low response time, large angle of incidence, and high spectral sensitivity at wide range of spectral emissions.

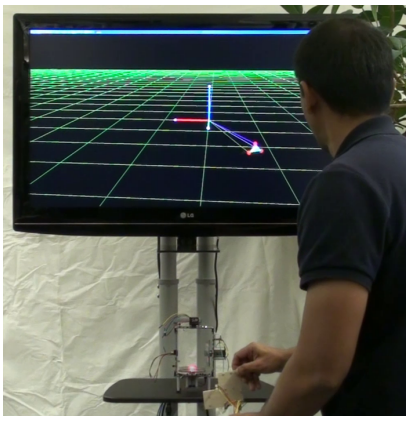

Fig. 6. Movement of the tracked object updates the 3D representation in real-time. The spacing between the green grid lines represents 20cm of distance in the real world.

Three of these photodiode sensor boards were attached to a flat surface as shown in Figure 5. All three photodiode sensor boards were connected to another circuit board containing the processing unit, which in this implementation was a Cortex M3 MCU (NXP LPC1313) microcontroller clocked at 72MHz. The microcontroller firmware was programmed to measure the azimuth and elevation angles of all the photodiodes in the triangular constellation as described in Section III-B. The processing unit board was connected to a PC via a USB connection, which was used to transfer the angle values as the photodiode signals were processed. Once the host PC received the angle values from the attached processing unit board, it performed the calculations described in Section III-C.

V. Results

The final 3D coordinates for each of the three sensors were rendered as a triangle in an OpenGL application, as shown in Figure 6. Moving the tracked object in all three movement axes and all three rotational axes while in the base station's scan volume (and while the photodiode sensors had line of

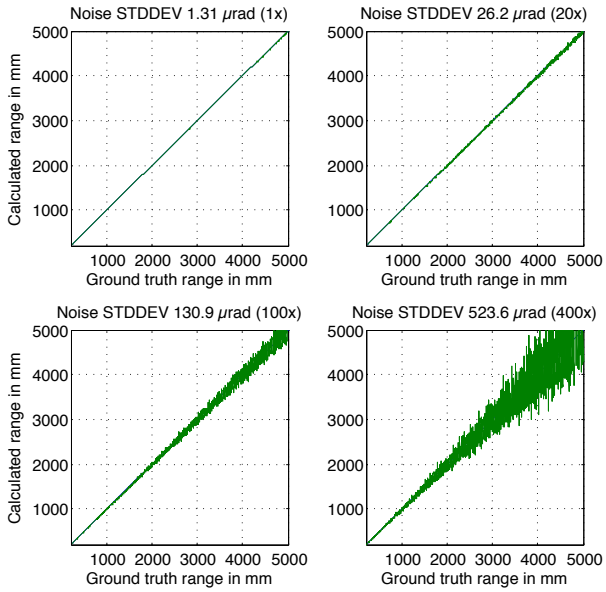

Fig. 7. The theoretical effect of the noisy measurements of the azimuth and elevation angles on the calculated range

sight to the base station) caused the 3D representation of the triangle to update in real-time.

The laser line sweeps are timed by the Cortex M3 microcontroller running at 72MHz. As the rotors spin at 15 Hz (900 RPM), the angular resolution of the azimuth and elevation measurements is 1.3089 microradians (7.4996×10^{-5} degrees). Figure 7 shows the theoretical effect of noise with standard deviation of 1x, 20x, 100x, and 400x measurement resolution on the range calculation.

When considering system noise, however, the standard deviation of the noise of the observed angular measurements of the implementation discussed in this paper fall between 300 to 400 times the measurement resolution. Most of this noise was introduced into the system by the mechanical vibrations caused by the slightly unbalanced rotors of the base station. The implemented system was able to determine the range of the photodiode constellation with a maximum error of 3 cm when the maximum distance between the base station and the constellation was around 1 meter. The average of the absolute errors between the calculated range and the ground truth from 30 cm to 5 meters of scan range for the system noise of different magnitude is given in Table I.

VI. Conclusion

This paper presented a unique low-cost indoor positioning system that consists of a base station emitting a fan of light that moves across the environment horizontally and vertically, thereby allowing photodiode sensors on the surface of a tracked object to determine their angles relative to the base station. By knowing the layout of the sensors on the object, Newton's iterative method was used to solve for the position and orientation of a three-sensor tracked object from the obtained angles. Since the tracked objects are independent

TABLE I
Average range error from ground truth for different measurement noise in a measurement range of 30cm to 5m

Angular Measurement Noise (Std. dev.)	Average Error (mm)
1x of measurement resolution = 1.31 μrad	0.3503
2x of measurement resolution = 2.62 μrad	0.7125
4x of measurement resolution = 5.24 μrad	1.3783
8x of measurement resolution = 10.5 μrad	2.8385
20x of measurement resolution = 26.2 μrad	7.0739
100x of measurement resolution = 130.9 μrad	35.5834
400x of measurement resolution = 523.6 μrad	139.1328

of the base stations, no limitation is placed on the number of objects that can be tracked within the range of the base station. As this method uses accurate time-based hardware events, the latency is less than other positioning systems, such as those based on vision sensors. While the calculated angular resolution that can be achieved by the system is very high, the results from a low-cost implementation showed that there is room for improvement. Future work will focus on managing the sources of jitter and noise throughout the system, such as by using low-jitter electrical and low-vibration mechanical components, as well as applying software-based filtering techniques on the tracking results.

References

[1] M. Abrash and D. Katz. (2014, May) Why Virtual Reality Isn't (Just) the Next Big Platform : Michael Abrash and Dov Katz of Oculus VR. Carnegie Mellon University Robotics Institute. [Accessed: October 2015]. [Online]. Available: https://www.youtube.com/watch?v=dxbh-TM5yNc

[2] O. Kreylos. (2014, October) Hacking the Oculus Rift DK2, part III. Doc-Ok.org. [Accessed: October 2015]. [Online]. Available: http://doc-ok.org/?p=1138

[3] G. Deak, K. Curran, and J. Condell, "A Survey of Active and Passive Indoor Localisation Systems," vol. 35, no. 16. Elsevier, 2012, pp. 1939–1954.

[4] A. Gruss, L. R. Carley, and T. Kanade, "Integrated Sensor and Range-Finding Analog Signal Processor," vol. 26, no. 3. IEEE Computer Society, 1991, pp. 184–191.

[5] R. Raskar, H. Nii, B. Dedecker, Y. Hashimoto, J. Summet, D. Moore, Y. Zhao, J. Westhues, P. Dietz, J. Barnwell *et al.*, "Prakash: Lighting Aware Motion Capture Using Photosensing Markers and Multiplexed Illuminators," in *ACM Transactions on Graphics (TOG)*, vol. 26, no. 3. ACM, 2007, p. 36.

[6] S. Linga, "A Novel Positioning System for Accurate Tracking in Indoor Environments," Master's thesis, Massachusetts Institute of Technology, 2007.

[7] (2013, February) The iGPS System. Amrikart. [Accessed: October 2015]. [Online]. Available: http://www.amrikart.com/infoletter-details/article/2013-02-11/The-iGPS-system/The-iGPS-system

[8] D. A. Maisano, J. Jamshidi, F. Franceschini, P. G. Maropoulos, L. Mastrogiacomo, A. Mileham, and G. Owen, "Indoor GPS: System Functionality and Initial Performance Evaluation," vol. 3, no. 3. Inderscience Publishers, 2008, pp. 335–349.

[9] J. Muelaner, Z. Wang, J. Jamshidi, and P. Maropoulos, "Verification of the Indoor GPS System by Comparison with Points Calibrated Using a Network of Laser Tracker Measurements," in *Proceedings of the 6th CIRP-sponsored international conference on digital enterprise technology*. Springer-Verlag, 2010, pp. 607–619.

[10] N. Chan and A. Yates. (2015, May) SteamVR's "Lighthouse" for Virtual Reality and Beyond. Tested. [Accessed: October 2015]. [Online]. Available: https://www.youtube.com/watch?v=xrsUMEbLtOs